Title	Ignition characteristics of 2-methyltetrahydrofuran: An experimental and kinetic study
Author(s)	Tripathi, Rupali; Lee, Changyoul; Fernandes, Ravi X.; Olivier, Herbert; Curran, Henry J.; Sarathy, S. Mani; Pitsch, Heinz
Publication Date	2016-10-10
Publication Information	Tripathi, Rupali, Lee, Changyoul, Fernandes, Ravi X., Olivier, Herbert, Curran, Henry J., Mani Sarathy, S., & Pitsch, Heinz. (2017). Ignition characteristics of 2-methyltetrahydrofuran: An experimental and kinetic study. Proceedings of the Combustion Institute, 36(1), 587-595. doi: https://doi.org/10.1016/j.proci.2016.07.103
Publisher	Elsevier
Link to publisher's version	https://doi.org/10.1016/j.proci.2016.07.103
Item record	http://hdl.handle.net/10379/6900
DOI	http://dx.doi.org/10.1016/j.proci.2016.07.103

Ignition characteristics of 2-methyltetrahydrofuran: An experimental and kinetic study

Rupali Tripathi[a], Changyoul Lee[b,c,*], Ravi X. Fernandes[b,d], Herbert Olivier[e], Henry J. Curran[c], S. Mani Sarathy[f], Heinz Pitsch[a]

[a]*Institute for Combustion Technology, RWTH Aachen University, 52056 Aachen, Germany*
[b]*Physico Chemical Fundamentals of Combustion, RWTH Aachen University, 52062 Aachen, Germany*
[c]*Combustion Chemistry Centre, National University of Ireland, Galway, Ireland*
[d]*Physikalisch Technische Bundesanstalt (PTB) Bundesallee 100, 38116 Braunschweig, Germany*
[e]*Shock Wave Laboratory, RWTH Aachen University, 52074 Aachen, Germany*
[f]*Clean Combustion Research Center, King Abdullah University of Science and Technology, Thuwal 23955-6900, Saudi Arabia*

Abstract

The present paper elucidates oxidation behavior of 2-methyltetrahydrofuran (2-MTHF), a novel second-generation biofuel. New experimental data sets for 2-MTHF including ignition delay time measurements in two different combustion reactors, i.e. rapid compression machine and high-pressure shock tube, are presented. Measurements for 2-MTHF/oxidizer/diluent mixtures were performed in the temperature range of $639 - 1413\,\mathrm{K}$, at pressures of 10, 20, and 40 bar, and at three different equivalence ratios of 0.5, 1.0, and 2.0. A detailed chemical kinetic model describing both low-and high-temperature chemistry of 2-MTHF was developed and validated against new ignition delay measurements and already existing flame species profiles and ignition delay measurements. The mechanism provides satisfactory agreement with the experimental data. For identifying key reactions at various combustion conditions and to attain a better understanding of the combustion behavior, reaction path and sensitivity analyses were performed.

Keywords: 2-Methyltetrahydrofuran, Ignition delay, Kinetic model, Shock tube, Rapid compression machine.

1. Introduction

The surge in energy demand and increased interest in climate and environmental issues over the last decades have contributed to the awareness that a sustainable energy source is necessary for economic and industrial growth, which has led to a strong interest for biofuels as alternative fuels. The use of first-generation biofuels is widely accepted as unsustainable due to the competition with the food supply. On the contrary, second-generation biofuels from non-feedstock materials, are seen as alternative sources for sustainable energy. Among second-generation biofuels, cyclic ethers have recently been recognized as potential candidates [1, 2]. An attractive alternative is 2-methyltetrahydrofuran, 2-MTHF, a second-generation biofuel [3–5], which has several advantages, such as high energy density compared to those of ethanol and gasoline, a lower heating value, which resembles that of gasoline and is higher than that of ethanol [6]. However, its octane rating is lower than that of ethanol and gasoline, which may limit its application as an additive [3, 7]. A spark-ignition engine study of Rudolph et al. [8] reveals the feasibility of 2-MTHF as a blending agent. Recently, a blend of 70% 2-MTHF with 30% di-*n*-butylether, was recognized as a fuel with optimum characteristics for diesel combustion [9], which tends to reduce particulate emission almost entirely in a single-cylinder diesel engine. Kar et al. [10] reported 2-MTHF as a component of p-series fuels, which are blends of ethanol, butanol, and 2-MTHF with higher alkanes, and are used to solve the cold start issues of pure ethanol fuels.

A strong interest in cyclic ethers as pure fuels as well as additives has resulted in many combustion studies of tetrahydrofuran (THF) [11–18]. These studies, however, have been limited to high temperatures. Research on 2-MTHF is scarce. Simmie et al. [2] computed bond dissociation energies (BDE) for C–H and C–C (carbon-methyl) bonds in 2-MTHF, barrier heights, and reaction enthalpies for all possible hydrogen-atom abstraction reactions by H atoms and methyl radicals at CBS-QB3 and G3 level of theory. Rate parameters of β-scission reactions from the initial α, β, and side-chain radicals were also computed. Chakravarty et al. [19] recently calculated the rate parameters for H-atom abstraction by hydroperoxyl radical employing CBS-QB3 and CCSD(T)/cc-pVTZ//B3LYP/cc-pVTZ levels of theory in the temperature range of $500 - 2000\,\mathrm{K}$. Moshammer et al. [20] presented a study of premixed, laminar, low-pressure flames of 2-MTHF at an equivalence ratio of 1.7 and a pressure of 40 mbar. Time-of-flight molecular-beam mass spectrometry (MBMS) with electron ionization (EI) was used for the investigation of species concentrations in the flames. A detailed model for high-temperature oxidation in low-pressure flames was also developed and validated against the species profiles of reactants, products, and important intermediates. Further, Wang et al. [21] in his high-temperature ignition delay times study of 2-MTHF utilized the model of Moshammer et al. [20] to predict experimental measurements.

In the present work, ignition delay measurements of 2-MTHF in a rapid compression machine (RCM) and a high-pressure shock tube (HPST) were performed, covering the low-to high-temperature regimes over a wide range of equivalence ratios and pressures. A detailed model was developed sys-

---

*Corresponding author:
Email address:* changyoul.lee@nuigalway.ie (Changyoul Lee)

tematically and validated against the novel and already available experimental results. The present study differentiates itself from other 2-MTHF kinetic model studies by including low-temperature kinetics for the first time.

2. Experimental approach

The ignition delay time experiments were performed in two different HPSTs and in RCMs. A brief description of the facilities and the experimental procedure for each of these facilities is provided in the following subsections. All experimental data along with the experimental conditions are provided in Table S1-S6 of the supplemental material.

2.1. NUI Galway high-pressure shock tube

The stainless steel shock tube used at NUI Galway has an inner diameter of 63.5 mm, a driver section of 3 m length, and a driven section of 5.7 m length described in detail in [22]. A diaphragm chamber, which houses two aluminium diaphragms is used to separate the driven and the driver section. The diaphragms are scored to the appropriate depth depending on the required pressure behind the reflected shock waves. The incident-wave velocities are measured using six PCB P113A piezoelectric pressure transducers mounted along the tube at 10, 150, 430, 710, 1025, and 2585 mm from the end wall of the driven section and an additional Kistler 603 B was mounted directly on the end-flange of the shock tube. The ignition delay time is defined as the time interval between the arrival of the incident shock at the end wall and the ignition event recorded by an abrupt pressure rise. In order to show the uniformity of ignition, a pressure trace from the measurements is provided in Fig. S1 of the supplemental material. The uncertainty of the temperature behind the reflected shock wave was estimated to be ±15 K.

2.2. RWTH Aachen high-pressure shock tube

The RWTH Aachen shock tube has a diameter of 14 cm, a driven section of 11 m, and a 4 m long driver section. This shock tube has been previously described in [23, 24]. Hence, only details relating to the present study are provided here. The ignition delay time is defined by the same method as used at NUI Galway. 2-MTHF/air mixtures were directly prepared in the test section of the shock tube by measuring the partial pressures of the vaporized 2-MTHF and synthetic air with typical mixture homogenization times of about an hour. All experimental data was acquired at a high sampling rate of 2.5 GHz. Ignition delay times were measured at an equivalence ratio of 1.0, temperatures ranging from 808 to 1103 K, and a nominal pressure of 10 and 20 bar. The estimated total uncertainty for the reflected shock temperature, T_5, is close to ±10 K.

2.3. NUI Galway rapid compression machine

The NUI Galway RCM, described in detail by Darcy et al. [25], was used to measure the ignition delay times at low-to-intermediate temperatures. This RCM is characteristically different from most other RCMs in that it has a twin-opposed piston configuration. Ignition delay time in RCM is defined as the

time difference between the end of compression and the highest pressure gradient. The adiabatic compression/expansion program of GasEq. [26] was used to calculate the compressed gas temperature and pressure. Pressure-time profiles were measured using a Kistler 601 A pressure transducer and transferred with a Kistler 5018 amplifier to the oscilloscope (Picoscope 4424). The initial temperature, pressure, and diluent compositions (N_2, Ar, and CO_2) were adjusted to vary the compressed temperature with a constant compressed pressure in the reaction chamber at the end of the compression. Ignition delay times were measured at $\phi = 0.5$, 1.0, and 2.0, temperatures ranging from 639 to 878 K, and compressed pressures of 10, 20, and 40 bar. Homogeneous fuel/air mixtures were prepared separately in a heated mixing tank. The estimated uncertainty of the measurements is ±5 K in compressed gas temperature. In order to illustrate the differences between the measurements performed at NUI Galway and at RWTH Aachen, typical pressure traces of RCM measurements from both facilities are presented in Fig. S2 of the supplemental material.

2.4. RWTH Aachen rapid compression machine

The heated RCM at RWTH Aachen University is described in detail by Lee et al. and Vrancks et al. [24, 27] at RWTH Aachen University. To vary the compressed-gas temperature, T_C, two approaches were used: 1) the proportions of the diluent gases (N_2/Ar) were adjusted to vary the overall heat capacities of the fuel and air mixture, 2) the compression ratios were varied between 14 ~ 31 through a unique construction of a movable end wall. For the current study, the reaction chamber was equipped with a thermal shock resistant Kistler 6125 C dynamic pressure transducer and a Kistler 5018 charge amplifier for pressure measurements during compression and any post-compression events, including ignition. The estimated uncertainty is ±4.5 K in compressed gas temperature. Gas mixtures were directly prepared in the reaction chamber and the mixture composition was determined by measuring the partial pressures of the gas-phase components. Ignition delay times were measured at $\phi = 1.0$, temperatures ranging from 648 to 771 K, and a compressed pressure of 20 bar.

3. Kinetic model development

3.1. Species nomenclature and bond nature

2-MTHF is a cyclic ether, containing four C atoms and one O atom in the ring along with one methyl side chain at the α to the O atom. Structure and BDEs of 2-MTHF are shown in Fig. 1. For the fuel specific species involved in the mechanism, C atoms are labeled numerically (i.e. 1, 2, 3) (Fig. 1). The site for the radical is labeled as j and the site for the double bond is labeled as * with the corresponding C number. The α tertiary C–H bond is the weakest bond among all C–H bonds in 2-MTHF followed by the α secondary C–H bond. The highest BDE occurs at the β primary C–H bond of the side chain. The reason for the lower BDE of the α C–H bond and higher BDE of the β C–H bond is the presence of the oxygen atom, which stabilizes the radical at α sites due to electron delocalization,
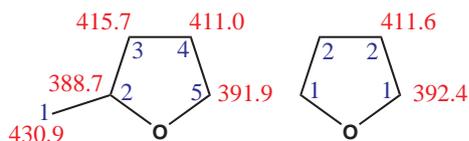
Figure 1: Structure and bond dissociation energies (in kJ/mol) of 2-MTHF, compared with those of THF [2]. The numbers in the blue, correspond to the carbon sites, and those in the red, correspond to the C–H bond dissociation energies.

while at β site this delocalization cannot take place, because the O atom is too far away [2]. The molecular structures of fuel-specific species along with their names are available in Table S7 of the supplemental material.

3.2. General model features

The mechanism development in the present work includes both high- and low-temperature chemistry of 2-MTHF, and includes the reactions known to be relevant in these temperature regimes. The model was built hierarchically upon the C_0–C_4 base model of Blanquart et al. [28]. The base mechanism has been extensively validated [29, 30] and contains the relevant chemistry needed to describe the oxidation of C_0-C_4 species. A sub-mechanism of 2-MTHF describing high-temperature specific reaction classes, was taken from the model of Moshammer et al. [20] and added to the base model.

C–H BDEs at α and β sites of THF are comparable to those of α and β sites on 2-MTHF (Fig. 1). Hence, the rate parameters for the reactions involving H-atom abstraction by $H\dot{O}_2$ and $\dot{O}H$ radicals for the secondary and tertiary sites were applied from the THF model of Tran et al. [18]. The rates for primary sites were taken from the optimized rates for alkanes [31] and the activation barrier was increased by 2 kcal/mol to include the BDE differences. Rate constants for H-atom abstraction by $H\dot{O}_2$, calculated theoretically by Chakravarty et al. [19], were not adopted here, because of their very low activation barriers, which lead to a vastly underpredicted reactivity as compared with experimental data. Some results are included in Fig. S3 of the supplemental material. Finally, a low-temperature sub-mechanism describing the oxidation of 2-MTHF at low temperatures was developed systematically on the basis of rate rules and reaction classes [32], and integrated with the other two parts of the mechanism. Twenty reaction classes describing low-temperature chemistry were added and rate parameters were applied from the optimized rate rules of Cai et al. [31]. Rate parameters were selected by comparing the BDEs of 2-MTHF with those of alkanes and the activation energy barrier was either decreased or increased according to the C–H BDE difference for the particular site at which the reaction takes place. Important modifications included in the mechanism were found to be consistent with the 2-butyltetrahydrofuran model of Cai et al. [33], and are as follows:

- The presence of the O atom in the ring decreases the C–H BDE at α centers; however, formed adducts at α centers, are less stable due to the weak bonding at these sites. A

similar trend is also seen in alcohols [34]. The rate parameters for O_2 addition at these sites were hence adopted from the butanol model of Sarathy et al. [34].

- Reaction rate constants for the $R\dot{O}_2$ to QOOH isomerization type of reactions (class 15) were adopted from the theoretical study of Parab et al. [35]. These rate parameters were calculated for all sites of 2-MTHF at CBS-QB3 level of theory.

- The prescribed rates for the second QOOH radical additions to O_2 (class 26) were estimated by analogy with fuel radical addition to O_2 (class 11) and divided by a factor of two as discussed by Bugler et al. [36].

- Various studies on cyclic hydrocarbons [37, 38] and higher tetrahydrofuran [33] revealed the need of high activation barriers for ketohydroperoxide decomposition reactions at low temperatures. Therefore, for the ketohydroperoxide decomposition reactions, an energy barrier of 41.6 kcal/mol was assigned from the methylcyclohexane study of Weber et al. [37].

- Isomerization of OOQOOH having OOH at tertiary α cannot take place through conventional pathways, because of the lack of the H atom at the tertiary center. Alternative pathways for these reactions were considered, as proposed in the iso-pentane model of Bugler et al. [36].

The developed reaction mechanism consists of 250 species and 2494 reactions (reverse and forward counted separately). Thermochemical data for each species considered in the mechanism were calculated using the THERM program [39], which uses the group additivity method of Benson [40]. Revised group additivity values [36] were considered for these calculations. The complete mechanism along with the thermochemical properties is available as supplemental material.

4. Results and discussion

This section presents the experimental results and validation of the numerical calculations. In order to attain a better understanding of the combustion behavior of 2-MTHF, rate of production (ROP) and sensitivity analyses were performed under the conditions of interest and all major pathways are discussed.

4.1. Experimental results and model validation

Ignition delay times measured in RCMs and STs are presented in Fig. 2. Figure 2a illustrates the effect of equivalence ratio on ignition delay times for 2-MTHF/oxidizer/diluent at 20 bar and at three different equivalence ratios of 0.5, 1.0, and 2.0. Figure 2b demonstrates the effect of pressure on ignition delay at $\phi = 1.0$ and at three different pressures of 10, 20, and 40 bar. The equivalence ratio was varied by changing the mole fraction of the fuel while keeping the mole fraction of O_2 constant at 20.4%. CHEMKIN-PRO code [41] and FlameMaster [42], along with the appropriate reactor selection, were used to perform numerical simulations. Both codes yield identical
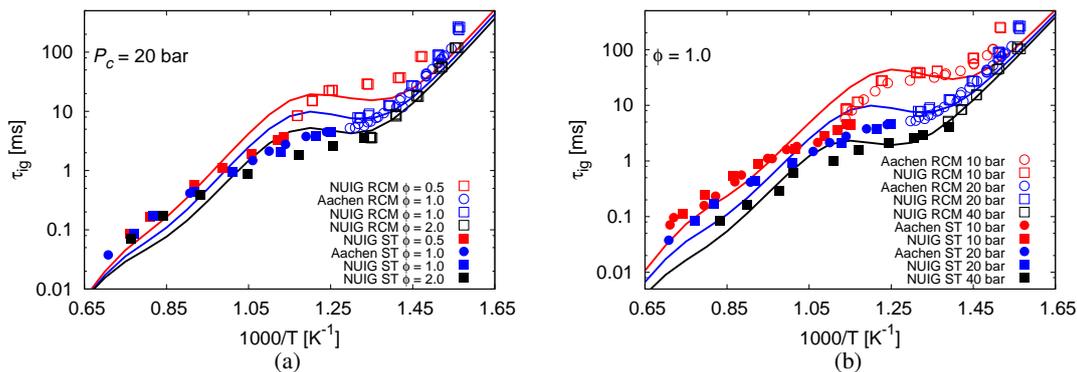
Figure 2: Ignition delay times of 2-MTHF/oxidizer/diluents, experimental data (points) and simulations at constant volume (lines) in RCM and in HPST; (a) effect of equivalence ratio; (b) effect of pressure.

numerical results. Simulations at constant volume are shown as line plots in Fig. 2. The experimental data indicate that increasing the equivalence ratio increases the reactivity of 2-MTHF across most of the temperature range investigated. The reactivity dependence on equivalence ratio can vary in different temperature regimes. Fuel reactivity is strongly sensitive to the equivalence ratio at intermediate temperatures, while it is less sensitive in the low- and high-temperature regions (Fig. 2a). This trend is similarly found also in the model predictions. When the equivalence ratio is kept constant and the pressure is varied, there is an increase in the reactivity of 2-MTHF when moving towards higher pressures (Fig. 2b). At constant temperature, it is clearly observed that increasing the pressure leads to a greater reactivity, which in turn leads to a decrease in ignition delay times. The experimental trend of increasing reactivity with equivalence ratio and pressure is reproduced well by the model.

In Fig. 2a and b, a linear Arrhenius dependence is seen in the region T >1090 K at 20 bar in both the measured data and in numerical simulations. In the temperature range of $690 - 1090$ K ($1.45 - 0.92$ K^{-1}), the ignition delay time increases nonlinearly with decreasing temperature. Upon decreasing the temperature further below 690 K (1.44 K^{-1}), the linear Arrhenius-type trend of increasing ignition delay times resumes. Such a behavior, which is typical for certain fuels, particularly alkanes indicates a negative temperature coefficient (NTC) [43, 44], even though it is weak for 2-MTHF. The NTC character of 2-MTHF increases with decreasing pressure and a similar behavior is reproduced by the model. The model captures ignition delay times in the intermediate temperature range reasonably well within the uncertainty limits of the experiments. However, in the high-temperature range ($1100 - 1428$ K ($0.91 - 0.70$ K^{-1})), it tends to be faster. At low temperatures, the model underpredicts the experimental data, because of the facility effect in the RCM. In RCMs, the pressure and temperature decrease in the reaction chamber after compression, due to heat loss to the cold combustion chamber walls. In order to account for these facility effects in the simulations, effective volume histories were used, which were derived from non-reactive pressure traces from the experiments. This method utilizes isentropic relations, in which
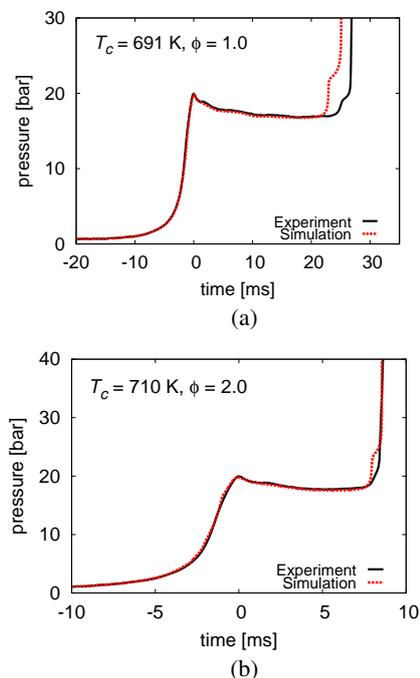

(a)

(b)

Figure 3: Comparison of experimental pressure traces to the calculated pressure traces at 20 bar.

the compression stroke is modeled as an isentropic compression and the facility effect during the post-compression phase on the adiabatic core of the cylinder volume is modeled as an isentropic volume expansion. The volume was calculated as a function of time for both the compression and end of compression phases, using the isentropic relations. Fig. 3 represents the comparison of pressure traces obtained from the measurements with the numerically calculated pressure traces at 20 bar, at two different equivalence ratios of 1.0 and 2.0 and for two temperatures at 760 K and 710 K, respectively. Good agreement is found at $\phi = 1.0$, but at $\phi = 2.0$ the model is slightly slower than the experiment at the investigated temperature of 691 K.

Thus, two types of simulations were performed: i) constant volume, i.e. adiabatic simulations represented as solid lines in
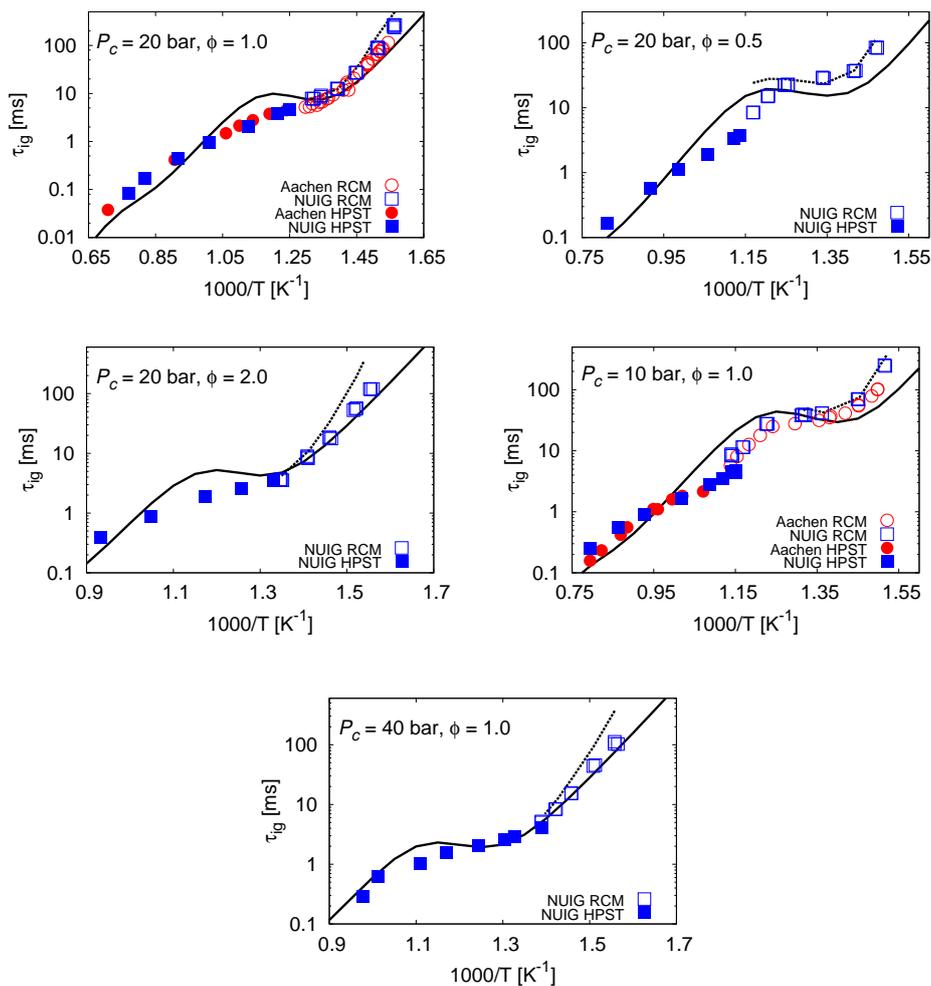
4

Figure 4: Ignition delay times for 2-MTHF/oxidizer/diluent, solid lines correspond to the simulation at constant volume and dashed lines correspond to the simulations including facility effect.

Fig. 4; and ii) simulations that account for the facility effects represented as dashed lines in Fig. 4. The proposed model predicts the experimental data fairly well at all pressures and over the complete temperature range. At 40 bar and $\phi = 1.0$ as well as at 20 bar and $\phi = 2.0$, the simulations slightly over-predict the measured data. More insight on the reactions dominating in these temperature regimes are discussed in the next section. In addition, the developed model was validated against the high-temperature, Ar-diluted ignition delay time measurements for 2-MTHF from Wang et al. [21] and against the species profile data from premixed laminar low-pressure flames of 2-MTHF from Moshammer et al. [20]. Good agreement is found between the calculated and experimental results. The performance of the model is shown in Fig. S4 and S5 of the supplemental material. In order to get further insight into the ignition behavior of 2-MTHF, the model was compared with the C_5 fuels n-pentanol [45] and n-pentane [36]. This highlights the effect of the ether functional group and the cyclic ring on auto-ignition. Simulated results are presented in Fig. S6 of the supplemental material. The ether functional group en-

hances the ignition propensity at high temperatures because of the lower C–H BDEs at α centers. As a consequence, 2-MTHF reacts faster than that of n-pentane and n-pentanol at high temperatures. However, at low temperatures, 2-MTHF reacts more slowly than the C_5 alkane, because of the presence of the cyclic ring hindering the low temperature specific isomerization pathways.

4.2. Reaction path and sensitivity analyses

A reaction path analysis of 2-MTHF oxidation is shown in Fig. 5. The flux analysis was carried out using constant volume, adiabatic simulations at two different temperatures of 1100 K and 650 K, and at a pressure of 20 bar for stoichiometric 2-MTHF/air mixtures. The first step in the consumption of 2-MTHF involves H-atom abstraction. 2-MTHF has five different carbon centers bearing H atoms. Although each of the five radicals are formed, fuel consumption predominantly takes place leading to the α-centered radicals because of the lower BDEs at these sites. Both α centers have comparable BDEs, but due to the two H atoms at the α secondary center, the production
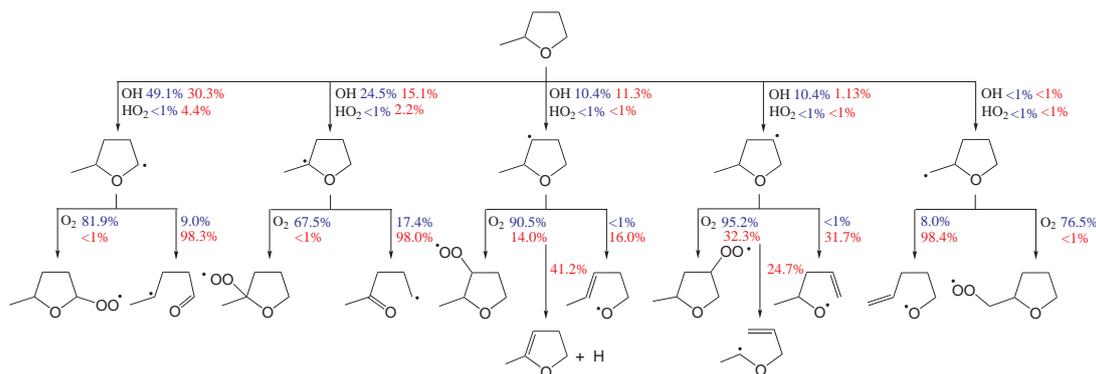
Figure 5: Simplified schematic of reaction path analysis for 2-MTHF/air mixtures at 30% fuel consumption at P = 20 bar, ϕ = 1, and at T = 650 K (blue numbers) and T = 1100 K (red numbers).

rate of the α secondary radical is twice as large as that of the α tertiary radical, which is consistent with the BDEs, reported by Simmie et al. [2]. However, fuel consumption leading to the β primary radicals is the slowest (less than 1%), since its BDEs are the highest among all the C–H bonds in 2-MTHF. At 650 K, the consumption takes place mainly because of H-atom abstraction by ȮH. When moving towards the high-temperature range, fuel consumption via H-abstraction by HȮ$_2$ also plays a minor role (Fig. 5). Further formed fuel radicals are predominantly consumed either via O$_2$ addition to the fuel radicals or through β-scission reactions. The relevance of fuel radical addition to O$_2$ reactions decreases with increasing temperature due to the onset of the competition with β-scission reactions, as seen in Fig. 5. At 650 K, the addition of fuel radicals to O$_2$ yielding RȮ$_2$ dominates over β-scission. On the contrary, at 1100 K, β-scission dominates over O$_2$ addition. The ring opening of fuel radicals predominantly takes place via C–O bond scission. This is due to the lower energy barrier for the C–O bond scission in comparison to the C–C bond [2]. On the contrary, the MTHF23J radical is predominantly consumed via α tertiary C–H bond scission at 1100 K, because of the thermodynamic stability of the formed product and a higher rate constant than that of the ring opening reactions as calculated by Simmie et al. [2]. At 650 K, the β fuel radicals predominantly undergo O$_2$ addition reactions. The consumption via the ring opening for such radicals is below 1%, while for the α fuel radicals it is slightly higher. The reason is that, due to the lower BDEs at α sites, ring opening reactions compete with those of the O$_2$ addition reactions.

A brute force sensitivity analysis (sensitivity factor of 2) was conducted to identify the reactions controlling ignition delay times and is presented in Fig. 6. The sensitivity analysis was performed for stoichiometric mixtures at the same conditions as considered in the reaction path analyses. A negative sensitivity implies an enhancement in reactivity, while reactions with positive sensitivity reduce reactivity and hence increase ignition delay. The most sensitive reactions, of all 2-MTHF consumption reactions, are those involving H-atom abstraction by ȮH radicals. At higher temperature, H-atom abstraction by HȮ$_2$ also becomes sensitive. Although the H-atom abstraction by HȮ$_2$ does not contribute much to the overall fuel consumption, it is
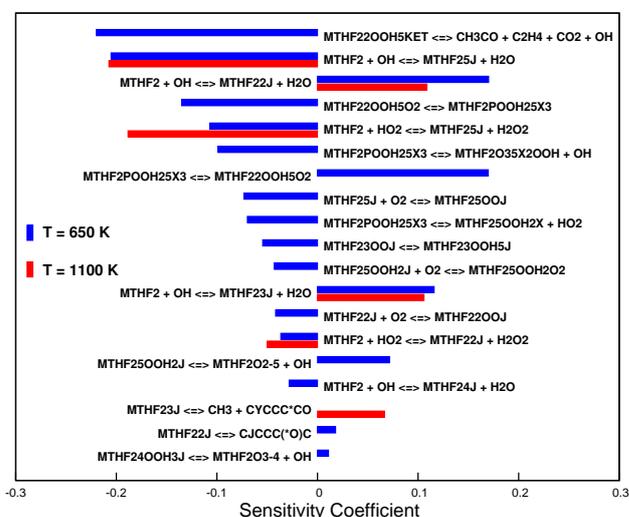

Figure 6: Sensitivity analysis on ignition delay of 2-MTHF/air mixtures at P = 20 bar and ϕ = 1.

very important for the early radical buildup at high-temperature and therefore has a high sensitivity coefficient. Consistent with the reaction path analyses, consumption of 2-MTHF radicals is most sensitive to addition to O$_2$ reactions, while at higher temperatures competition with the β-scission reactions is observed. Regarding fuel radical chemistry at 650 K, the sensitivity of radical addition to O$_2$ reactions, isomerization of RȮ$_2$ to QOOH, second isomerization reactions of OOQOOH, and ketohydroperoxide reactions, is evident from the sensitivity diagram. The RȮ$_2$ to QOOH reaction takes place predominantly via a 6-membered transition state because it has the lowest barrier, as explained in the recent study of Parab et al. [46]. For the α tertiary radical, also the reaction involving isomerization to the β center via 6-membered transition state, yielding P(OOH)$_2$, is seen to show negative sensitivity. Decomposition of P(OOH)$_2$ is sensitive to the reaction forming a cyclic ether and ȮH, because of the lower barrier of this reaction in comparison to the ring opening reaction [36]. At the conditions studied, a competition between the cyclic ether formation and

isomerization reactions for $R\dot{O}_2$ consumption is observed. This hinders low-temperature branching and hence increases the ignition times. In addition to that, sensitivity analyses were also performed in the NTC ignition regime at a temperature of 800 K and at two different pressures of 10 and 20 bar. For the sake of brevity, these results are shown in Fig. S7 of the supplemental material. The sensitivity analysis confirms that reactions involving H-atom abstraction by $H\dot{O}_2$ and $\dot{O}H$ have a significant effect on 2-MTHF ignition at the intermediate temperature of 800 K. Addition of fuel radicals to O_2 also plays an important role at the studied conditions.

5. Conclusions

The present study reports the first low-temperature, experimental, and chemical kinetic study of 2-MTHF. A detailed mechanism was developed and employed to simulate the oxidation behavior of 2-MTHF against the new experimental data and the literature data. The ignition delay time measurements were performed in HPSTs and in RCMs, at temperatures between 639 and 1413 K, at pressures of 10, 20, and 40 bar, and at three equivalence ratios of 0.5, 1.0, and 2.0. Good agreement was observed between the ignition delay data measured in HPSTs and RCMs and also between the ignition delay data obtained in these facilities at two different locations. The overall reactivity of the 2-MTHF oxidation is well-predicted by the model. 2-MTHF experiments show a slight NTC behavior, which was also reproduced by the model. The dependence of fuel reactivity on the pressure and the equivalence ratio was also investigated. It was observed that an increase in pressure or fuel concentration enhances the reactivity of 2-MTHF. This trend was observed at all the pressures and equivalence ratios investigated and was well reproduced by the numerical simulations.

Reaction flux and sensitivity analyses were performed to understand the consumption and oxidation of 2-MTHF. It appears that the reactions involving H-atom abstraction by $\dot{O}H$ are the most dominating pathways for the consumption of the fuel. A theoretical calculation study for these reactions will improve model performance and reduce the predictive uncertainties. The current investigation, provides a significant contribution to the understanding of oxidation of the simplest alkyltetrahydrofuran and provides a base for higher tetrahydrofurans.

References

[1] M. Thewes, M. Muether, S. Pischinger, M. Budde, A. Brunn, A. Sehr, P. Adomeit, J. Klankermayer, Energy Fuels 25 (2011) 5549–5561.
[2] J.M. Simmie, J. Phys. Chem. A 116 (2012) 4528–4538.
[3] J.-P. Lange, E. van der Heide, J. van Buijtenen, R. Price, ChemSusChem 5 (2012) 150–166.
[4] W. Yang, A. Sen, ChemSusChem 3 (2010) 597–603.
[5] G.W. Huber, S. Iborra, A. Corma, Chem. Rev. 106 (2006) 4044–4098.
[6] L.S. Tran, B. Sirjean, P.-A. Glaude, R. Fournet, F. Battin-Leclerc, Energy 43 (2012) 4–18.
[7] E. Christensen, J. Yanowitz, M. Ratcliff, R.L. McCormick, Energy Fuels 25 (2011) 4723–4733.
[8] T.W. Rudolph, J.J. Thomas, Biomass 16 (1988) 33–49.
[9] A.J. Janssen, F.W. Kremer, J.H. Baron, M. Muether, S. Pischinger, J. Klankermayer, Energy Fuels 25 (2011) 4734–4744.
[10] Y. Kar, H. Deveci, Energy Sources Part A 28 (2006) 909–921.
[11] C.H. Klute, W.D. Walters, J. Am. Chem. Soc. 68 (1946) 506–511.
[12] G. McDonald, N.M. Lodge, W.D. Walters, J. Am. Chem. Soc. 73 (1951) 1757–1760.
[13] A. Lifshitz, M. Bidani, S. Bidani, J. Phys. Chem. 90 (1986) 3422–3429.
[14] M.J. Molera, A. Couto, J.A. Garcia-Dominguez, Int. J. Chem. Kinet. 20 (1988) 673–685.
[15] P. Dagaut, M. McGuinness, J.M. Simmie, M. Cathonnet, Combust. Sci. Technol. 135 (1998) 3–29.
[16] T. Kasper, A. Lucassen, A.W. Jasper, W. Li, P.R. Westmoreland, K. Kohse-Höinghaus, B. Yang, J. Wang, T.A. Cool, N. Hansen, Z. Phys. Chem. 225 (2011) 2237–1270.
[17] Y. Uygun, S. Ishihara, H. Olivier, Combust. Flame 161 (2014) 2519–2530.
[18] L.S. Tran, M. Verdicchio, F. Monge, R.C. Martin, R. Bounaceeur, B. Sirjean, P.-A. Glaude, M.U. Alzueta, F. Battin-Leclerc, Combust. Flame 162 (2015) 1899–1918.
[19] H.K. Chakravarty, R.X. Fernandes, J. Phys. Chem. A 117 (2013) 5028–5041.
[20] K. Moshammer, S. Vranckx, H.K. Chakravarty, P. Parab, R.X. Fernandes, K. Kohse-Höinghaus, Combust. Flame 160 (2013) 2729–2743.
[21] J. Wang, X. Wang, X. Fan, K. Yang, SAE Technical Paper 2015-01-1807 (2015).
[22] D. Darcy, M. Mehl, J.M. Simmie, J. Würmel, W.K. Metcalfe, C.K. Westbrook, W.J. Pitz, H.J. Curran, Proc. Combust. Inst. 34 (2013) 411–418.
[23] S. Vranckx, K.A. Heufer, C. Lee, H. Olivier, L. Schill, W.A. Kopp, K. Leonhard, C.A. Taatjes, R.X. Fernandes, Combust. Flame 158 (2011) 1444–1455.
[24] C. Lee, S. Vranckx, K.A. Heufer, S.V. Khomik, Y. Uygun, H. Olivier, R.X. Fernandes, Z. Phys. Chem. 226 (2011) 1–27.
[25] D. Darcy, H. Nakamura, C.J. Tobin, M. Mehl, W.K. Metcalfe, W.J. Pitz, C.K. Westbrook, H.J. Curran, Combust. Flame 161 (2014) 65–74.
[26] C. Morley, GasEq. http://www.gaseq.co.uk.
[27] S. Vranckx, C. Lee, H.K. Chakravarty, R.X. Fernandes, Proc. Combust. Inst. 34 (2013) 377–384.
[28] G. Blanquart, P. Pepiot-Desjardins, H. Pitsch, Combust. Flame 156 (2009) 588–607.
[29] K. Narayanaswamy, G. Blanquart, H. Pitsch, Combust. Flame 157 (2010) 1879–1898.
[30] K. Narayanaswamy, P. Pepiot, H. Pitsch, Combust. Flame 161 (2014) 866–884.
[31] L. Cai, H. Pitsch, S.M. Sarathy, S.Y. Mohamed, V. Raman, J. Bugler, H.J. Curran, Optimized reaction mechanism rate rules for normal alkanes, Combust. Flame in press.
[32] S.M. Sarathy, C.K. Westbrook, M. Mehl, W.J. Pitz, C. Togbé, P. Dagaut, H. Wang, M.A. Oehlschlaeger, U. Niemann, K. Seshadri, P.S. Veloo, C. Ji, F.N. Egolfopoulos, T. Lu, Combust. Flame 158 (2011) 2338–2357.
[33] L. Cai, H. Minwegen, J. Beeckmann, U. Burke, R. Tripathi, A. Ramalingam, A. Sudholt, J. Klankermayer, K.A. Heufer, H. Pitsch, Experimental and numerical study of a novel biofuel: 2-butyltetrahydrofuran, Proc. Combust. Inst. submitted.
[34] S.M. Sarathy, P. Oßwald, N. Hansen, K. Kohse-Höinghaus, Prog. Energy Combust. Sci. 44 (2014) 40–102.
[35] P.R. Parab, N. Sakade, Y. Sakai, R.X. Fernandes, K.A. Heufer, Computational kinetic study on ROO to QOOH reactions in 2-methyltetrahydrofuran oxidation, in preparation.

[36] J. Bugler, K.P. Somers, E.J. Silke, H.J. Curran, J. Phys. Chem. A 119 (2015) 7510–7527.

[37] B.W. Weber, W.J. Pitz, M. Mehl, E.J. Silke, A.C. Davis, C.-J. Sung, Combust. Flame 161 (2014) 1972–1983.

[38] K. Narayanaswamy, H. Pitsch, P. Pepiot, Combustion and Flame 162 (2015) 1193–1213.

[39] E.R. Ritter, J.W. Bozzelli, Int. J. Chem. Kinet. 23 (1991) 767–778.

[40] S.W. Benson, Thermochemical kinetics, Wiley, 1976.

[41] Reaction Design, Inc. CHEMKIN-PRO Release 15101; Reaction Design, Inc.: San Diego, CA, 2010.

[42] H. Pitsch, Flamemaster: A C++ Computer Program for 0D Combustion and 1D Laminar Flame Calculations, 1993.

[43] R. Minetti, M. Ribaucour, M. Carlier, L.R. Sochet, Combust. Sci. Technol. 113 (1996) 179–192.

[44] M. Carlier, C. Corre, R. Minetti, J.-F. Pauwels, M. Ribaucour, L.-R. Sochet, Symp. (Int.) Combust. 23 (1991) 1753–1758.

[45] K.A. Heufer, S.M. Sarathy, H.J. Curran, A.C. Davis, C.K. Westbrook, W.J. Pitz, Energy Fuels 26 (2012) 6678–6685.

[46] P.R. Parab, N. Sakade, Y. Sakai, R.X. Fernandes, K.A. Heufer, J. Phys. Chem. A 119 (2015) 10917–10928.